Journal of Asian Earth Sciences 42 (2011) 123–133

Contents lists available at ScienceDirect

Journal of Asian Earth Sciences

journal homepage: www.elsevier.com/locate/jseaes

Exhumation of the Dahinggan Mountains, NE China from the Late Mesozoic to the Cenozoic: New evidence from fission-track thermochronology

Xiaoming Li [a,*], Xiaoyong Yang [b], Bin Xia [a], Guilun Gong [a], Yehua Shan [a], Qiaosong Zeng [a], Wei Li [a], Weidong Sun [a]

[a] Key Laboratory of Mineralogy and Metallogeny, Guangzhou Institute of Geochemistry, Chinese Academy of Sciences, Guangzhou 510640, China
[b] School of Earth and Space Sciences, University of Science and Technology of China, Hefei 230026, China

ARTICLE INFO

Article history:
Received 15 October 2010
Received in revised form 28 March 2011
Accepted 19 April 2011
Available online 27 April 2011

Keywords:
Fission-track
Exhumation
The Dahinggan Mountains
Late Mesozoic–Cenozoic
Geodynamics

ABSTRACT

Zircon and apatite fission-track (FT) analyses were used to reveal the exhumation of Phanerozoic granitoid intrusions in the Dahinggan Mountains, northeastern China. Zircon FT ages ranging from 84 ± 5 to 97 ± 8 Ma, and apatite FT ages from 47 ± 3 to 67 ± 4 Ma with mean track lengths between 12.3 ± 2.3 and 13.3 ± 2.2 μm, respectively, were obtained for the Phanerozoic granitoids sampled along a south–south-west to north–north-east transect across the Dahinggan Mountains. Three cooling stages from the Late Mesozoic to the Cenozoic have been identified in the studied region based on FT results and modeling. Stage one was a rapid cooling period from the closure temperature of zircon FT to the high temperature part of the apatite FT partial annealing zone (~210–110 °C) during ~90–57 Ma. Stage two was a relatively slow cooling period (~110–60 °C) occurred between ~57 Ma and 20 Ma, suggesting that the granitoids had been exhumed to depths of ~1–2 km. The final stage was a cooling period (60–20 °C) occurred since the Miocene, which bring studied samples to the Earth's surface at an accelerated exhumation rate. The estimated maximum exhumation is ~5 km assuming a steady-state geothermal gradient of 35 °C/km. Our results indicate that this exhumation is possibly led by the Pacific plate subduction combined with intracontinental orogeny associated with asthenospheric upwelling.

1. Introduction

The northeastern (NE) China together with its neighboring regions is the eastern segment of the gigantic accreting continental margin of the Mongolia-Okhotsk orogenic belt (Fig. 1a). Since the Late Paleozoic, it has undergone long-term plate subduction and continent-arc and/or microcontinent–continent collisions before the ultimate collision between the North China-Mongolian Block and the Siberian Craton (Zhao et al., 1990, 1994; Sengör et al., 1993; Van der Voo et al., 1999; Xiao et al., 2003; Jia et al., 2004; Li, 2006). Consequently, widespread Phanerozoic granitoids were formed in NE China and along the north margin of North China Block (Wu et al., 2000, 2002, 2003, 2005; Jahn et al., 2001; Sun et al., 2001; Meng, 2003; Hong et al., 2004). In the eastern segment of the accreting continental margin, it is proposed that the Mongolia–Okhotsk Ocean diminished and ultimately closed in the Early Cretaceous, which marked the final accretion of the East Asian continent (Zonenshain et al., 1990; Ma and Yang, 1993).

The NE China together with its neighboring regions has become part of the circum-Pacific tectonomagmatic belt since the Late Mesozoic. It is still controversial as regarding to the relationship between the extensive magmatic activities in NE China (probably throughout the East China) and the Paleo-Pacific Ocean subduction after intensive studies (Lapierre et al., 1997; Xu et al., 1999; Li, 2000; Yin et al., 2000; Zhou and Li, 2000; Fan et al., 2003; Deng et al., 2004; Wu et al., 2005; Li and Li, 2007). Moreover, the exhumation process of the NE China after the collision is poorly understood.

Phanerozoic granitoids, mainly formed in the Late Jurassic to the Early Cretaceous, are widely cropped out in the Dahinggan Mountains, NE China (Shao et al., 1998a, 1999; Wu et al., 2000, 2002, 2003, 2005, 2011; Jahn et al., 2001) (Fig. 1b), suggesting that the rocks overlying these granitoids have largely been unroofed or denuded. The total exhumation since the Late Mesozoic was on kilometer scale.

In contrast to epicontinental and intercontinental orogeny, intracontinental orogeny is controlled by deep-seated factors, for example, asthenospheric upwelling. There are two contrasting explanations for the exhumation of the Dahinggan Mountains: vertical accretion due to underplating and the effect of the indispensable equilibrium process in the intracontinental orogeny model (e.g., Shao et al., 1998b, 2005) vs. the Pacific plate subduction after the Late Cretaceous indicated by the reflective data of geophysics (Engebretson et al., 1985; Northrup et al., 1995). Therefore, the

* Corresponding author. Address: 511 Kehua Street, Wushan, Guangzhou 510640, China. Tel.: +86 20 85290123; fax: +86 20 85290130.
E-mail address: lixm@gig.ac.cn (X. Li).

1367-9120/$ - see front matter © 2011 Elsevier Ltd. All rights reserved.
doi:10.1016/j.jseaes.2011.04.014

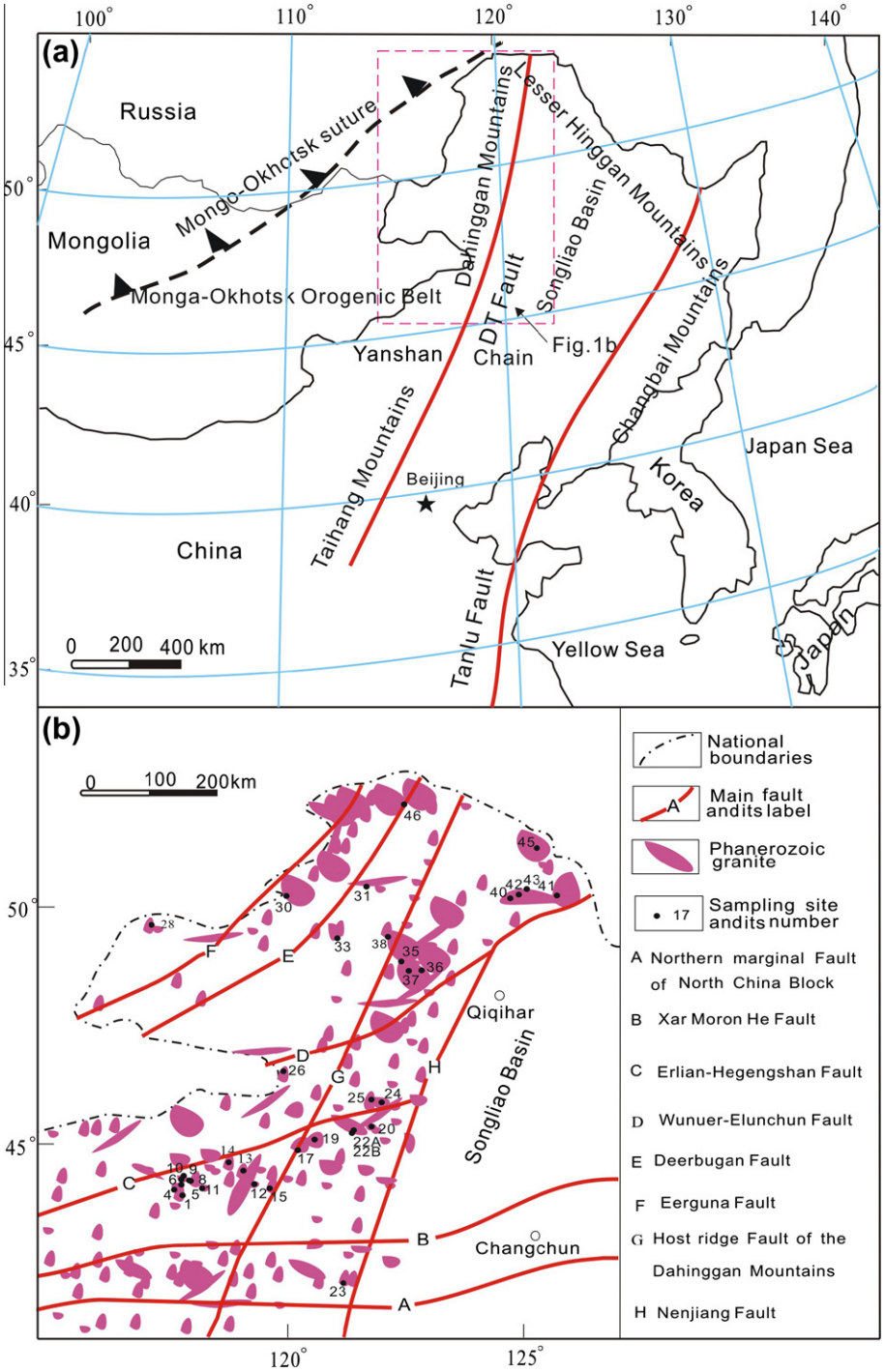

Fig. 1. (a) Sketch map of the Mongo-Okhotsk orogenic belt, showing the study area; and (b) Sketch map of Phanerozoic granotoids of the Dahinggan Mountains, showing the locations of surface samples (modified after BGMRNM (1991)). *Note*: Faults A–H are regional deep faults conjectured with geophysical features and field outcrops (BGMRNM, 1991). Among them, A is the boundary fault between northern China Block and Mongo-Okhotsk orogenic belt; B is the plate subduction suture in the early Paleozoic; C is the suture between the Siberia plate and the North China plate in the later Paleozoic; D is a fault inside the Siberia plate in the later Paleozoic; E is a fault inside the Siberia plate in the later Proterozoic to early Paleozoic; F is a fault inside the Siberia plate in the Paleozoic; G is northern part of DT Fault formed in the Mesozoic which represents by the gravity gradient across the whole Dahinggan Moutains; H is the boundary fault between the Dahinggan Mountains and the Songliao Basin.

Dahinggan Mountains is an ideal candidate for understanding the subsequent exhumation process in NE China together with its neighboring regions. The age and exhumation rate of the Dahinggan Mountains were, however, not well constrained.

Fission-track (FT) dating is an effective method to reveal the history of the exhumation and the pattern of tectonic geomorphology in the upper crust, which has been successfully applied to studies on the spatial and temporal patterns of the exhumation since the Mesozoic in the Alps, Appalachians, Andes, Qinghai-Tibetan Plateau, the ultrahigh pressure Qingling-Dabie-Sulu belt, etc. (e.g., Gleadow and Fitzgerald, 1987; Kemp, 1989; Wagner and Van den haute, 1992; Fitzgerald and Stump, 1997; Johnson, 1997; Gallagher et al., 1998; Roden-Tice et al., 2000; Grimmer et al., 2002; Willett et al., 2003; Yuan et al., 2006; Vassallo et al.,

2007; Tinker et al., 2008; Wang et al., 2009; Li et al., 2010; Li and Gong, in press). In this study, we use zircon and apatite FT analyses to better constrain the age and cooling rate of the Dahinggan Mountains and provide firmer constraints on their exhumation history. The data are also used to establish the Late Mesozoic–Cenozoic tectonic geomorphology and evolution of the Dahinggan Mountains, deciphering the influence of the Pacific plate subduction (e.g., Li and Li, 2007; Sun et al., 2007) on the Late Mesozoic–Cenozoic tectonic evolution in NE China and neighboring regions.

2. Geological setting

The north–north-east trending Dahinggan Mountains, located near the border of China, Russia and Mongolia, are just obliquely bestriding the Hinggan-Mongolia orogen, and are also distantly opposite the Taihang Mountains with the Yanshan Chain in-between, both depicting the main tectonic framework of East China (Fig. 1a). They are more than 1000 km long, hundreds of kilometer wide, and more than 2000 m above the sea level in the southwest decreasing gradually to hundreds of meters above the sea level in the northeast (Fig. 1b). Their Moho becomes deeper gradually westward, with an abrupt change in crust thickness of 35–36 km in the east to ~46 km in the west (BGMRNM, 1991). It is the north part of the famous Dahinggan Mountains–Taihangshan Mountains (DT) gravity gradient belt, which is one of the most important structural belts in eastern China (Xu, 2007).

The latterly formed NNE trending Dahinggan Mountains–Taihangshan Mountains (DT) Fault, approximately distributed along the host ridge of the Dahinggan Mountains, cuts all of the pre-existing, large-scale faults, including the Northern Marginal Fault of North China Block, the Xar Moron He Fault, and the Erlian–Hegenshan Fault. These pre-existing faults control the distribution of Yanshanian (from the Jurassic to the Cretaceous) igneous rocks, but have no evident displacement along them (Liu et al., 2004; Xu, 2007) (Fig. 1b).

More than 75% area of the Dahinggan Mountains is covered by the Mesozoic magmatite, forming a significant polymetallic ore belt in NE China, with important resources of tin, copper, lead, and zinc (Liu et al., 2004). The intensive magmatic activities and regional granitoid emplacement in the middle-southern Dahinggan Mountains are mainly concentrated during 150–120 Ma, 150–140 Ma and 140–120 Ma, respectively. Most of the granitoid intrusions in the northern Dahinggan Mountains are emplaced from the late Paleozoic to the Late Cretaceous, with only a small number formed in the Proterozoic or the Early Paleozoic (BGMRNM, 1991; BGMRHLJ, 1993).

The Mesozoic mantle upwelling of the Dahinggan Mountains has continued until the Cenozoic. However, large scale eruptions of basalt, with mantle xenoliths, are mainly distributed in the rifting valleys of the Cenozoic basins, especially those on the sides of the Dahinggan Mountains (Liu et al., 1992, 2001; Wang et al., 2002; Lei and Zhao, 2005). Thus, they probably have insignificant influence on the tectonic uplift of the Dahinggan Mountains.

3. Sampling and experimental methods

Thirty-five representative samples of fresh Phanerozoic granitoids from a south-south-west to north–north-east transect across the Dahinggan Mountains, in this study, were collected for FT analysis (Fig. 1b, Table 1). Most samples are of the Jurassic to the Early Cretaceous in age, with a few samples of the Carboniferous, the Permian or the Triassic (Table 1). These samples are fine- to coarse-grained granite or diorite, without any significant tectonic or magmatic overprinting. Efforts have been paid to avoid possible thermal effect related to active faults and/or Cenozoic magmatisms.

In addition, we measured the longitude and latitude of each sampling location using a portable GPS with precision in the order of 10 m, along with its elevation with precision in the order of 5 m. This sampling strategy allows comparing the distribution of the FT ages with the relative elevations of the granitoids in order to estimate the variations in the cooling rates, and the inferred exhumation rates.

Apatite and zircon grains were obtained by crushing, sieving, magnetic and heavy liquids separation techniques. Apatite and zircon grains were mounted by epoxy resin and FEP (fluroethylene-propylene) Teflon sheets, respectively. These prepared samples were carefully ground and polished to an optical finish to expose internal grain surfaces. Apatite spontaneous fission tracks were revealed by 5.5 M HNO_3 at 21 °C for 20 s (Carlson et al., 1999), and zircon by a molten 8 g NaOH + 11.5 g KOH eutectic at 220 °C for 20–60 h (Gleadow et al., 1976), as necessary to obtain a high-quality etch (Gleadow, 1981).

Zircon and apatite FT ages were analyzed by using external detector method (Hurford and Green, 1983). The mounts were covered with a flake of low-U muscovite, packed for irradiation, together with standard uranium dosimeter glass SRM612 and standard known age sample FCT (27.8 ± 0.7 Ma) (Hurford and Green, 1983), and irradiated in a well-thermalized (Cd for Au > 100) neutron flux 492 Swim reactor, Chinese Institute of Atomic Energy. After irradiation, muscovites were etched in 40% HF at 25 °C for 20 min to reveal induced fission tracks. Maximum etch pit dimensions (Dpar) were concurrently monitored as a representative of their chlorine content. Only those crystals with prismatic sections parallel to the *c*-crystallographic axis were accepted for Dpar analysis, because of their high etching efficiency. The FT ages were calculated following the method recommended by Hurford (1990), using the zeta calibration method (Hurford and Green, 1983). Ages were calculated using the Trackkey software® (Dunkl, 2002). Ages quoted are central fission track ages with one standard error. Zeiss Axioplan microscope at 1250× magnification with AUTOSCAN system was used to observe and measure the spontaneous and induced densities of zircon and apatite FT populations, as well as confined lengths and their related Dpar values of apatite fission tracks.

4. Results

4.1. FT data

The central ages of zircon and apatite FT (as zircon and apatite FT ages in this study), the mean track lengths (MTL) and the mean Dpar values of apatite FT are listed in Table 1, whilst the representative plots of apatite FT length distributions are illustrated in Fig. 2. The measured zircon and apatite FT ages range from 84 ± 5 to 97 ± 8 Ma and 47 ± 3 to 67 ± 4 Ma, respectively (Table 1). All the measured apatite FT lengths are unimodal in distribution (Fig. 2), with a mean length of 12.3–13.3 μm and a standard deviation of ca. 2.0 μm, and a mean Dpar value of 1.5 ± 0.2 μm to 2.4 ± 0.3 μm (Table 1).

To better interpret the significance of our data, we modeled six representative apatite FT data sets with a large number of track lengths to quantify the timing and amount of cooling at specific locations. Their time–temperature paths most likely reveal the exhumation history of the Dahinggan Mountains due to the six samples basically evenly distributing in the Dahinggan Mountains (Fig. 1b).

Time–temperature histories were calculated using the inverse modeling approach of HeFty (Ketcham, 2005) with a multi-

Table 1
Fission-track data of the Dahinggan Mountains.

Sample No./ mineral	Longitude E	Latitude N	Elevation (m)	Rock type	Formation era*	*n*	ρ_s/ $\times10^5$ cm^{-2} (N_s)	ρ_i / $\times10^5$ cm^{-2} (N_i)	ρ_d/ $\times10^5$ cm^{-2} (N_d)	Central age (Ma)	$P(\chi^2)$ (%)	Mean track length ± 1σ/μm	No. of tracks	Mean Dpar ± 1σ/μm
DH1–Ap	117°40.390′	43°12.490′	1030	Granite	J_1–K_1	30	11.9 (557)	22.8 (1068)	5.8 (5815)	51 ± 3	95	12.4 ± 1.5	33	1.7 ± 0.2
DH1–Zr						6	89.7 (897)	21.9 (219)	1.3 (3290)	88 ± 7	97			
DH4–Ap	117°25.693′	43°36.550′	1540	Moyite	J_3	13	11.2 (517)	21.5 (992)	5.8 (5815)	51 ± 3	95			
DH4–Zr						7	136.3 (1022)	34.7 (260)	1.4 (4125)	89 ± 7	99			
DH5–Ap	117°31.310′	43°57.254′	1750	Monzogranite	J_1–K_1	24	7.7 (360)	15.8 (743)	5.8 (5211)	47 ± 3	94	12.7 ± 1.5	21	1.5 ± 0.2
DH5–Zr						10	89.2 (2361)	21.6 (566)	1.3 (3290)	90 ± 5	95			
DH6–Ap	117°33.195′	43°58.334′	1728	Granite	J_1–K_1	13	11.4 (149)	21.8 (286)	5.9 (5723)	52 ± 5	95			
DH6–Zr						7	129.4 (1375)	32.1 (341)	1.3 (3290)	87 ± 6	99			
DH8–Ap	117°55.968′	43°51.680′	1090	Granodiorite	J_1–K_1	14	8.4 (126)	16.5 (247)	5.8 (5815)	50 ± 6	82			
DH8–Zr						12	60.3 (1318)	14.6 (319)	1.3 (3290)	89 ± 6	100			
DH9–Ap	117°53.389′	43°46.827′	1110	Diorite	J_1–K_1	11	17.0 (255)	35.9 (537)	5.9 (5723)	47 ± 4	88			
DH9–Zr						10	148.8 (1207)	36.7 (298)	1.3 (3290)	87 ± 6	99			
DH10–Ap	117°55.113′	43°44.775′	1035	Granite porphyry	J_1–K_1	20	4.4 (196)	9.0 (406)	5.9 (5723)	48 ± 4	57			
DH10–Zr						6	153.6 (960)	37.8 (236)	1.3 (3290)	88 ± 7	99			
DH11–Ap	118°05.985′	43°25.074′	960	Granite	J_1–K_1	20	17.2 (431)	34.8 (871)	5.9 (5723)	49 ± 3	97	13.0 ± 1.4	30	1.6 ± 0.2
DH11–Zr						5	59.3 (741)	15.3 (191)	1.4 (4125)	88 ± 8	99			
DH12–Ap	119°18.519′	43°49.367′	659	Granite	J_1–K_1	20	16.3 (1236)	29.1 (2200)	5.8 (5815)	55 ± 3	95	12.3 ± 2.3	106	1.8 ± 0.4
DH12–Zr						7	305.2 (1717)	74.5 (419)	1.3 (3290)	88 ± 6	100			
DH13–Ap	119°09.439′	44°14.994′	633	Monzonite	J_1–K_1	20	10.6 (258)	18.5 (450)	5.8 (5211)	56 ± 5	95			
DH13–Zr						7	128.9 (1047)	31.9 (259)	1.3 (3290)	87 ± 7	99			
DH14–Ap	118°53.374′	44°28.550′	1050	Diorite	T_3–J_3	25	11.9 (476)	17.7 (709)	5.8 (5211)	66 ± 4	98			
DH14–Zr						8	157.0 (883)	39.8 (224)	1.3 (3290)	85 ± 7	100			
DH15–Ap	119°15.530′	44°12.950′	619	Granite	J_1–K_1	30	11.4 (793)	19.5 (1349)	5.8 (5211)	57 ± 3	98			
DH15–Zr						10	90.2 (620)	21.7 (149)	1.3 (3290)	90 ± 9	100			
DH17–Ap	120°24.513′	44°56.340′	635	Granodiorite	J_1–K_1	10	12.2 (229)	21.3 (355)	5.9 (5723)	64 ± 6	97			
DH17–Zr						8	128.8 (805)	33.0 (206)	1.4 (4125)	89 ± 8	91			
DH19–Ap	120°28.677′	45°26.966′	836	Riebeckite granite	J_3–K_1	20	11.2 (307)	22.7 (623)	5.9 (5723)	49 ± 4	98			
DH19–Zr						8	136.8 (855)	34.0 (212)	1.3 (3290)	87 ± 7	100			
DH20–Ap	121°40.643′	45°58.153′	448	Diorite	T–J	10	29.3 (458)	58.0 (906)	5.8 (5211)	49 ± 3	76			
DH20–Zr						7	120.2 (526)	31.5 (138)	1.4 (4125)	87 ± 9	93			
DH22A–Ap	121°01.218′	45°27.788′	478	Quartz diorite	P_2	25	13.1 (742)	21.0 (1192)	5.8 (5815)	61 ± 3	100	12.7 ± 1.8	68	1.9 ± 0.2
DH22A–Zr						10	147.3 (1381)	36.9 (346)	1.3 (3290)	86 ± 6	100			
DH22B–Ap				Granodiorite		20	11.3 (333)	18.0 (529)	5.9 (5723)	63 ± 5	95	12.7 ± 1.5	40	2.1 ± 0.2
DH22B–Zr						12	129.8 (1703)	33.2 (436)	1.3 (3290)	84 ± 5	100			
DH23–Ap	121°09.688′	41°50.577′	268	Diorite	J_1–K_1	30	10.4 (291)	17.9 (503)	5.8 (5815)	57 ± 5	99			

DH23–Zr						10	148.0 (925)	32.8 (205)	1.3 (3290)	97 ± 8	100			
DH24–Ap	121°28.928′	46°13.551′	389	Granite	T	12	12.0 (158)	23.2 (305)	5.8 (5815)	51 ± 5	84			
DH24–Zr						8	100.4 (1695)	25.8 (436)	1.3 (3290)	84 ± 5	98			
DH25–Ap	121°17.714′	46°18.198′	435	Granite	J_1–K_1	25	18.3 (1325)	33.7 (2446)	5.8 (5815)	53 ± 2	35	13.0 ± 2.0	78	1.6 ± 0.2
DH25–Zr						8	106.3 (1262)	25.4 (302)	1.3 (3290)	90 ± 7	100			
DH26–Ap	119°45.791′	47°18.925′	867	Granite	J_3	15	6.47 (295)	12.08 (551)	5.75 (5211)	52.2 ± 4.1	97			
DH26–Zr						5	109.2 (1706)	28.7 (448)	1.4 (4125)	87 ± 5	99			
DH28–Ap	117°37.891′	49°30.303′	652	Quartz monzonite	J_1–K_1	20	7.8 (356)	15.2 (695)	5.8 (5211)	50 ± 4	99	12.5 ± 1.5	30	150 ± 0.2
DH28–Zr						5	104.6 (654)	26.6 (166)	1.3 (3290)	85 ± 8	100			
DH30–Ap	119°43.265′	50°32.230′	730	Monzogranite	P_2	20	28.6 (1357)	44.9 (2131)	5.8 (5815)	63 ± 3	49	13.3 ± 2.2	94	2.4 ± 0.2
DH30–Zr						12	96.2 (1624)	25.8 (436)	1.4 (4125)	85 ± 5	98			
DH31–Ap	121°29.585′	50°46.260′	723	Granite porphyry	J_1–K_1	20	13.5 (505)	22.3 (836)	5.9 (5723)	60 ± 4	90			
DH31–Zr						8	152.5 (1231)	37.3 (303)	1.3 (3290)	88 ± 6	94			
DH33–Ap	121°01.549′	49°05.053′	698	Monzogranite	T	22	10.6 (694)	17.4 (1144)	5.9 (5723)	60 ± 3	69	12.7 ± 2.0	65	2.4 ± 0.3
DH33–Zr				porphyry		13	139.4 (1568)	34.5 (388)	1.3 (3290)	87 ± 6	97			
DH35–Ap	122°46.319′	48°00.191′	354	Hornblende	K_1	25	9.6 (585)	14.0 (858)	5.8 (5211)	67 ± 4	98			
DH35–Zr				monzogranite		10	229.3 (2580)	59.1 (665)	1.3 (3290)	84 ± 5	72			
DH36–Ap	122°51.076′	47°33.399′	353	Alkaline granite	K_1	17	8.6 (109)	15.3 (191)	5.8 (5211)	55 ± 7	98			
DH36–Zr						10	125.6 (1570)	28.7 (359)	1.3 (3290)	94 ± 6	95			
DH37–Ap	122°35.824′	47°33.299′	349	Porphyritic granite	T	20	12.1 (311)	20.8 (532)	5.8 (5815)	58 ± 4	99	12.7 ± 1.6	33	2.1 ± 0.2
DH37–Zr						7	26.0 (699)	6.5 (174)	1.3 (3290)	87 ± 8	100			
DH38–Ap	122°21.645′	47°45.147′	414	Granodiorite	J_1– K_1	25	11.8 (776)	24.0 (1572)	5.8 (5815)	49 ± 3	27	12.3 ± 1.9	56	1.7 ± 0.2
DH38–Zr						5	162.8 (814)	42.6 (213)	1.4 (4125)	87 ± 7	100			
DH40–Ap	124°07.185′	50°25.320′	403	Moyite	T	25	9.3 (370)	19.3 (771)	5.8 (5815)	58 ± 4	99	12.7 ± 1.8	45	2.0 ± 0.2
DH40–Zr						6	9.6 (657)	2.5 (169)	1.4 (4125)	88 ± 8	97			
DH41–Ap	125°41.437′	50°33.785′	463	Biotite	K_1	28	6.2 (343)	10.7 (589)	5.8 (5815)	57 ± 4	99			
DH41–Zr				monzogranite		7	116.6 (1094)	29.2 (274)	1.3 (3290)	86 ± 7	98			
DH42–Ap	124°16.441′	50°35.421′	459	Plagiogranite	J_3– K_2	20	12.7 (866)	21.1 (1438)	5.8 (5211)	59 ± 3	23	12.8 ± 2.0	63	2.0 ± 0.2
DH42–Zr						5	123.2 (1001)	30.5 (248)	1.3 (3290)	87 ± 7	88			
DH43–Ap	124°18.531′	50°42.601′	426	Monzogranite	P	30	5.5 (366)	9.2 (612)	5.8 (5815)	59 ± 4	98	13.1 ± 1.9	53	1.9 ± 0.2
DH43–Zr						10	29.3 (1647)	7.2 (404)	1.4 (4125)	93 ± 6	99			
DH45–Ap	124°41.045′	52°19.707′	378	Monzogranite	C	20	48.8 (1229)	69.9 (2052)	5.8 (5815)	59 ± 3	95	12.9 ± 1.7	55	2.0 ± 0.2
DH45–Zr						7	221.5 (2077)	54.1 (507)	1.4 (4125)	93 ± 6	93			
DH46–Ap	122°28.722′	52°59.160′	507	Diorite porphyry	T	20	20.6 (1544)	31.9 (2394)	5.9 (5723)	64 ± 3	94	13.3 ± 2.1	83	2.2 ± 0.2
DH46–Zr						6	125.3 (1644)	29.9 (393)	1.4 (4125)	95 ± 6	95			

Note: n – number of crystals counted; ρ_s – spontaneous track density of a sample; N_s – number of tracks counted to determine ρ_s; ρ_i – induced track density of a sample measured in a muscovite external detector; N_i – number of tracks counted to determine ρ_i; ρ_d – induced track density of glass dosimeter SRM612 measured in a muscovite external detector; N_d – number of tracks counted to determine ρ_d; $P(\chi^2)$ – probability of equaling or exceeding χ^2 $(n-1)$ degrees of freedom; $*$ – (after BGMRNM (1991) and BGMRHLJ (1993)). Ages determined by external detector method using zeta values of 340.8 ± 8.5 and 331.5 ± 9.6 for apatite and zircon, respectively.

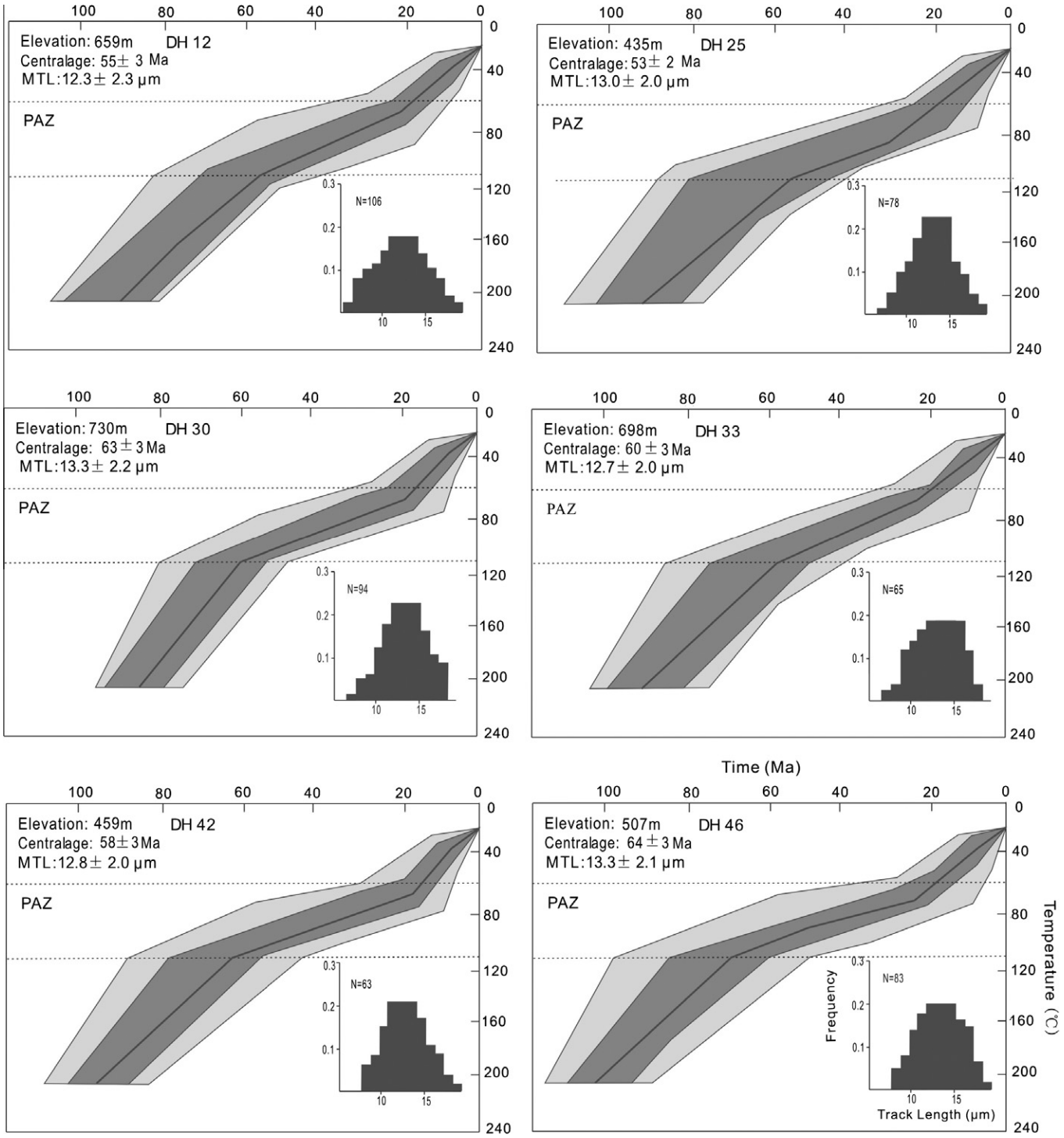

Fig. 2. Representative plots of time–temperature paths modeled by the apatite FT data and distributions of apatite FT lengths in the Dahinggan Mountains. Legends are given at the last pair of the figure. Thermal modeling of apatite FT length and age data modeled time–temperature paths for six apatite samples, computed with HeFty program by Ketcham (2005). Temperature ranges between 110 and 60 °C delineate apatite partial annealing zone, defined as temperature interval in which majority of track length shortening take place. Additionally, several conditions are as follows: (1) the present day temperature is set to a constant value of 20 °C; (2) kinetic variable of Dpar was input; (3) temperature ranges between 210 and 110 °C were constrained by zircon and apatite FT ages; and (4) modeling scheme was Monte Carlo. We modeled 10,000 paths for each plot. Thick lines show best-fit solutions obtained for these model run, and dark-gray and light-gray colors show good-fit solutions and accept-fit solutions obtained for same model run, respectively.

compositional annealing model (Ketcham et al., 2007b) and the Dapr value as kinetic parameter. Models were run using *c*-axis projected lengths (Ketcham et al., 2007a), and initial track lengths were calculated according to the mean Dpar value of each sample using the formula of Carlson et al. (1999). The thermal history modeling results are illustrated in Fig. 2.

4.2. Cooling history analysis of each sample

The probability of equaling or exceeding χ^2 $(n-1)$ degrees of freedom of FT ages, or $P(\chi^2)$, is far greater than 5% (Table 1), indicating that the ages of zircon and apatite crystals can be classified as single population for each sample.

The measured FT ages (<100 Ma) are markedly younger than the formation ages of the host-rocks (>100 Ma) (BGMRNM, 1991; BGMRHLJ, 1993; Wu et al., 2011). Therefore, they represent the cooling ages of the samples during the uplift and denudation processes because of their negligible effects from magmatic or tectonic activities since the Late Cretaceous (BGMRNM, 1991; BGMRHLJ, 1993).

The apatite samples have experienced significant track annealing and a relatively long-term lingering in the apatite FT partial annealing zone owing to the evident shortening of apatite fission tracks (Table 1).

In Fig. 2, the modeling time–temperature cooling curves exhibit multi-stages or episodic patterns, including two rapid and one slow cooling in the Dahinggan Mountains since the Late Mesozoic.

4.3. Comparison of exhumation history among various locations

Table 1 shows similar age patterns of zircon and apatite FT in different sampling locations, suggesting a simple exhumation pattern for the Dahinggan Mountains since the Late Mesozoic, i.e., similar onset time and exhumation rate at different locations. However, the FT age vs. elevation plot (Fig. 3a) manifests the weak

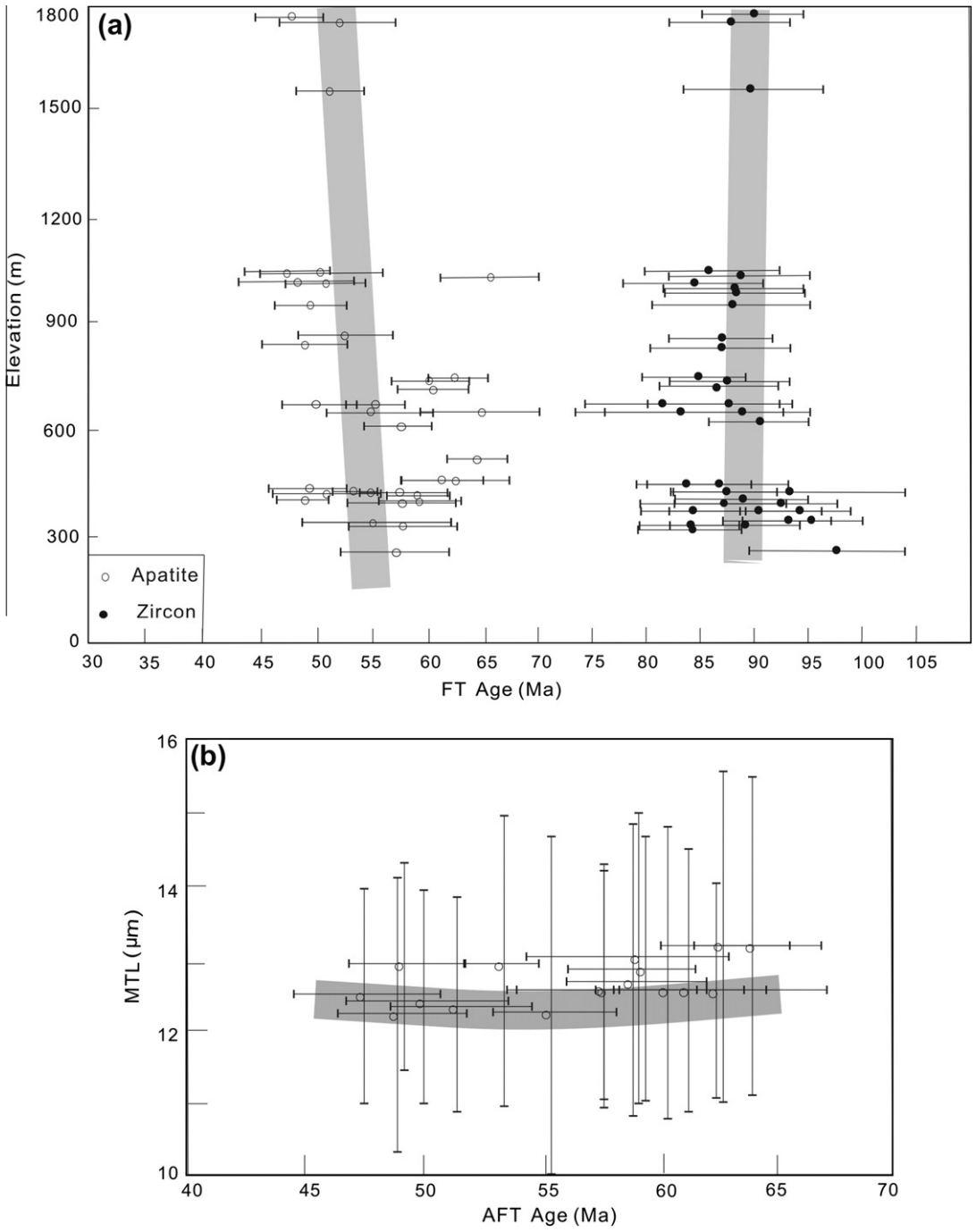

Fig. 3. Plot of (a) FT ages vs. elevations, and (b) AFT ages vs. MTLs (mean apatite FT lengths). Error bar represents ±1σ. The data show no clear relationship between FT age and sample elevation as would be expected from simple exhumation of a region of low topographic relief, as well as inferior boomerang plots for AFT age vs. MTL.

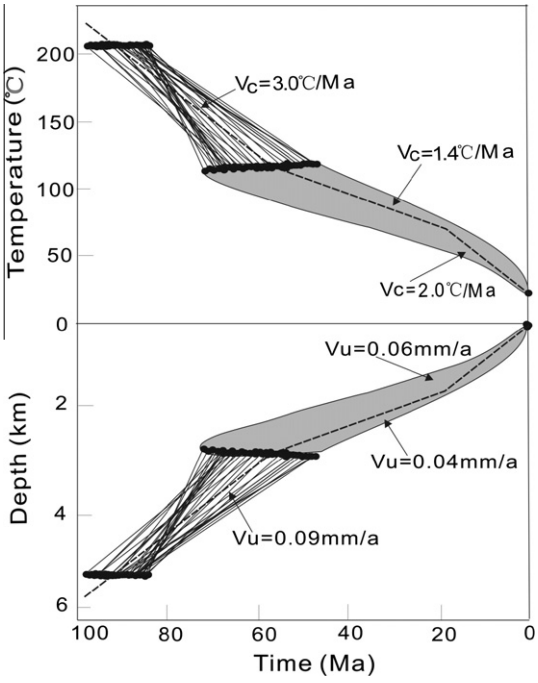

Fig. 4. Sketch map of the cooling, and inferred exhumation history in the Dahinggan Mountains since the Late Mesozoic. The data denote an episodic cooling, and inferred exhumation, under a steady-state geothermal gradient of 35 °C/km, in the Dainggan Mountains since the Late Mesozoic.

relationship between age and sample elevation, not as would be expected from a region experiencing simple exhumation, as well as inferior boomerang plots for AFT (apatite FT) age vs. MTL (Fig. 3b). This may have resulted from the compositional effect of the apatite FT data (e.g., Barbarand et al., 2003; Vassallo et al., 2007) due to some difference of the mean Dpar values (1.5 ± 0.2–2.4 ± 0.3 μm) (Table 1).

The zircon and apatite FT ages suggest that these samples once cooled to the closure temperatures of zircon and apatite FT, and exhumed to the equivalent burying depths during ~84–97 Ma and ~47–67 Ma, respectively.

To the east, the Songliao Basin has the average geothermal gradient of 37 °C/km in the present-day, decreasing gradually outward to ~30 °C/km, all less than the paleogeothermal gradient in the basin (Ren, 1999). Thus, we can assume that the steady-state geothermal gradient was 35 °C/km in the Dahinggan Mountains.

Fig. 4 synthetically illustrates the cooling, and inferred exhumation history, under a steady-state geothermal gradient of 35 °C/km, in the Dainggan Mountains since the Late Mesozoic. It has probably experienced an episodic cooling, and inferred exhumation in the Dahinggan Mountains since the Late Mesozoic as follows:

(1) The first rapid cooling rate of ~3.0 °C/Ma, and inferred exhumation rate of ~0.09 mm/a during ~90–57 Ma by using zircon and apatite "mineral pair" FT ages vs. their closure temperatures.
(2) Subsequent slow cooling rate of ~1.4 °C/Ma, and inferred exhumation rate of ~0.04 mm/a during ~57–20 Ma by apatite FT modeling.
(3) A second rapid cooling rate of ~2.0 °C /Ma, and inferred exhumation rate of ~0.06 mm/a since ~20 Ma by deducing from samples' cooling starting from the low temperature of apatite FT partial annealing.

5. Discussion

The FT analyses performed within the Dahinggan Mountains allowed us to reconstruct their exhumation history and deduce their exhumation geodynamics over the period the Late Mesozoic to Recent time.

5.1. Episodic exhumation

An episodic exhumation in a range of 0.04–0.09 mm/a in the Dahinggan Mountains since the Late Mesozoic was obtained from FT thermochronology (Fig. 4). The similar zircon and apatite FT ages of all the samples means that they were exhumed through the partial annealing zone of zircon and apatite FT as a simple orogen, and the main upper part of the Dahinggan Mountains remained at temperatures lower than ~210 °C, ~110 °C and ~60 °C after cooling episode in ~90, ~57 and ~20 Ma, respectively. Under a steady-state paleogeothermal gradient of 35 °C/km as discussed previously, the present surface of the Dahinggan Mountains should have been buried at a depth of ~5–6, ~2–3 and ~1–2 km in the period of the Late Cretaceous, Early Paleogene, and Early Neogene periods, respectively.

The results show that the maximum exhumation is likely ~5.0 km in the Dahinggan Mountains since the Late Mesozoic (Fig. 4). However, the current elevation is more than 2000 m above the sea level in the southwest, and decreases gradually to hundreds of meters above the sea level in the northeast of the Dahinggan Mountains, and the Dahinggan Mountains have been characterized by continental deposits since the Early Mesozoic (BGMRHLJ, 1993). Thus, this suggests a magnitude of at least 3–4 km for the total unroofing in the Dahinggan Mountains since the Late Mesozoic, based on the relationship among surface uplift, uplift of rocks and exhumation of rocks (England and Molnar, 1990).

Regional evolution since the Late Cretaceous was probably related to the Farallon- Izanagi and Kula-Pacific ridges subduction toward the NE Asian continental margin (Engebretson et al., 1985; Northrup et al., 1995; Taira, 2001), and the time of Izanagi–Farallon ridge subduction into NE China may be between 106 and 55 Ma, and basically fit for the movement track of the Pacific Plate and Eurasian Plate from paleogeomagnetism data (Zhao and Coe, 1996; Guo et al., 2007). The peneplain and differential vertical uplift-subsidence movements mainly occurs in the Northeastern Asian during the Paleogene, and rifting of the northeastern margin of the Asian continent started at ~22 Ma and was followed by development of the Japan Sea Basin, which separated from the Asian continent between 22 and 15 Ma (Nakamura et al., 1990; Taira, 2001). Back-arc extension continued into the Quaternary, associated with the central eruption style of the Neogene-Quaternary basaltic lavas in NE China (e.g. Basu et al., 1991; Liu et al., 2001; Lei and Zhao, 2005). Apatite FT data from the Songliao Basin, adjacent to the Dahinggan Mountains, indicate that the late stage tectonic movements in the Songliao Basin have zoning in space and episodes in time (Xiang et al., 2007). Clearly, the episodic exhumation of the Dahinggan Mountains since the Late Mesozoic is consistent with these geological processes. Furthermore, integrated with the whole Cenozoic stratigraphic sequences, and structural inversion in the Songliao Basin (Ren, 1999), these sedimentary records also reflect the episodic exhumation of the Dahinggan Mountains during the Late Mesozoic–Cenozoic. Therefore, the FT data and modeling are reliable.

5.2. Exhumation geodynamics

If the Late Mesozoic–Cenozoic episodic exhumation of the Dahinggan Mountains was simply caused by the Pacific plate

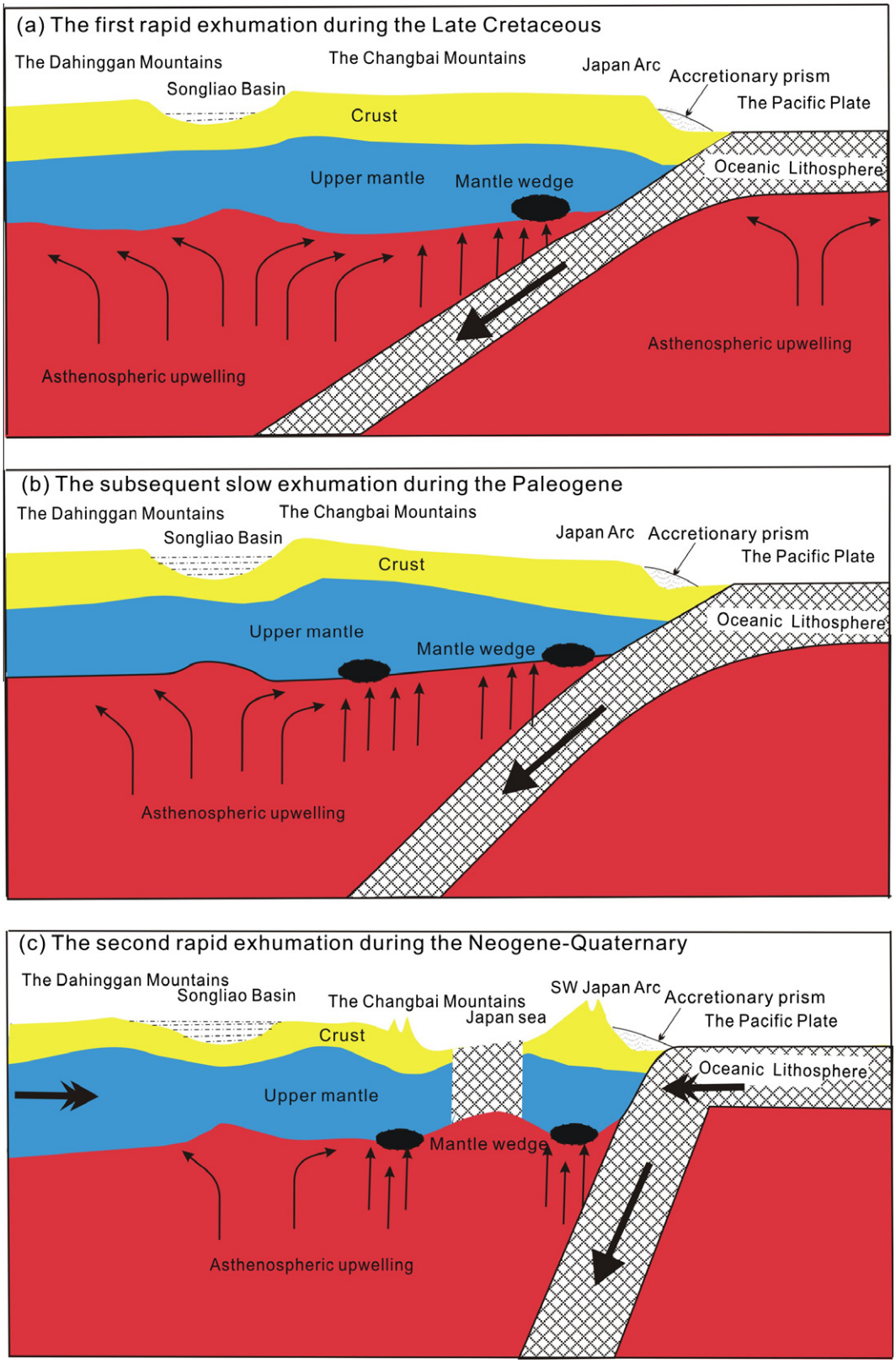

Fig. 5. Cartoons for the episodic exhumation of the Dahinggan Mountains since the Late Mesozoic. (a) The first exhumation during the Late Cretaceous, (b) the subsequent slow exhumation during the Paleogene, and (c) the second rapid exhumation during the Neogene-Quaternary. (See text for details.)

subduction beneath the Eurasian Plate, the far-field effect of the Pacific plate subduction would lead to that the onset of the exhumation occurred in the Late Mesozoic, and that the FT ages became younger westwards gradually in the Dahinggan Mountains. However, because the collision between North China and Siberia around 160 Ma obstructed the westwards movement of the lithosphere induced by the Pacific plate subduction, which caused the thickened lithospheric delaminating from west edge of the northeast China-Mongolia block at ~160 Ma and extended gradually eastwards. Mantle upwelling and underplating resulted in

volcanism migrating from the west to the east in northeastern Asia during the Late Mesozoic (Wang et al., 2006). Consequently, the onset time of the exhumation seemed to occur later as FT ages became younger eastwards gradually in the Dahinggan Mountains.

Hence, we could deduce that the onset time of exhumation was at least varied, possibly resulted in the dissimilar FT ages in the west and the east of the Dahinggan Mountains. However, neither diverse FT ages nor conspicuous deformation of the exposed granitoids occurred in the west and the east of the Dahinggan Mountains, and the exhumation appears to be simple since the Late Mesozoic.

In case the exhumation of the Dainggan Mountains was just caused by the intracontinental orogeny associated with asthenospheric upwelling, it seemed to be able to better explain how the pattern of shallow basin-mountain responded to the deep geological processes, and the basalt eruption occurred in the rift basins, but inconveniently interpret how such episodic exhumation as well as geodynamical mechanism of the Dahinggan Mountains has taken place since the Late Mesozoic.

Therefore, we propose a combination of the Pacific plate subduction and the intracontinental orogeny associated with asthenospheric upwelling that better accounts for the uplift and denudation of the Dahinggan Mountains since the Late Mesozoic. The scenario of the three-stage exhumation is described below.

(1) The first rapid exhumation and contemporary magmatic activity during the Late Cretaceous (~90–57 Ma) were caused by the intracontinental orogeny associated with asthenospheric upwelling, as a result of the subduction of the Farallon–Izanagi and Kula- Pacific ridges toward the NE Asian continental margin (Fig. 5a).
(2) Subsequent slow exhumation during the Paleogene (~57–20 Ma) was the postorogenic uplift and denudation process, mainly caused by the post-subduction extension in the region (Fig. 5b).
(3) The second rapid exhumation under the compression regime during the Neogene and Quaternary (~20–0 Ma) was predominantly controlled by the subduction of the Pacific plate beneath the Eurasia Plate (Fig. 5c).

This model does not only provides a better explanation for the characteristics of FT data, but are compatible with the occurrence of the intracontinental orogeny of the Dahinggan Mountains, and magmatic activities closely related to the Pacific plate subduction (Lin et al., 1998; Ge et al., 1999; Shao et al., 1999, 2005; Wu et al., 2000, 2005; Deng et al., 2004; Lei and Zhao, 2005). Further, this study allows us to understand the tectonic geomorphology and its evolution of the Dahinggan Mountains since the Late Mesozoic, whilst it offers new isotopic geochronology to recognize the evolution of the NE China and neighboring regions since the Late Mesozoic.

This model, however, suggests that the Late Mesozoic–Cenozoic exhumation of the Dahinggtan Mountains is markedly distinct from that of the Yanji area in the east of Songliao Basin, mainly led by the subduction of the Pacific plate beneath the Eurasian Plate (Li et al., 2010), and slightly different from that of the Lesser Hinggan Mountains in the northeast of Songliao Basin, resulted from the Pacific plate subduction combined with intracontinental orogeny associated with asthenospheric upwelling (Li and Gong, in press). This implies the varied exhumation history of different regions in NE China together with neighboring regions.

6. Conclusions

Zircon and apatite FT ages and thermal history modeling results reveal that the Dahinggan Mountains have experienced a three-stage cooling history spanning the Late Mesozoic and Cenozoic eras. Two distinct periods (~90–57 Ma and ~20–0 Ma) of rapid cooling, and inferred exhumation history can be identified from zircon and apatite FT ages, and modeling time–temperature paths, respectively. The slow cooling, and inferred exhumation history between the two rapid exhumation processes of ~57–20 Ma can be recognized from apatite FT ages and modeling. As this exhumation process can not simply be ascribed either to the Pacific plate subduction or to the intracontinental orogeny, we believe that their combination can better explain the exhumation of the Dahinggan Mountains since the Late Mesozoic.

Acknowledgements

We thank two anonymous reviewers and Prof. Bor-ming Jahn for their constructive comments and suggestion, which are helpful for us to improve the manuscript significantly. This work was financially supported by the National Natural Science Foundation of China (Grant Nos. 40572124, 41072158 and 90814008). This is contribution NO. 1332 from GIGCAS.

References

Barbarand, J., Carter, A., Wood, A., Hurford, A.J., 2003. Compositional and structural control of fission track annealing in apatite. Chemical Geology 198, 107–137.
Basu, A.R., Wang, J.W., Huang, W.K., Xie, G.H., Tatsumoto, M., 1991. Major element, REE, and Pb, Nd and Sr isotopic geochemistry of Cenozoic volcanic rocks of eastern China: implications for their origin from suboceanic-type mantle reservoirs. Earth and Planetary Science Letters 105, 149–169.
Bureau of Geology, Mineral Resources of Heilongjiang Province (BGMRHLJ), 1993. Regional Geology of Heilongjiang Province. Geological Publishing House, Beijing (in Chinese with English abstract).
Bureau of Geology, Mineral Resources of Nei Mongolia Autonomous Region (BGMRNM), 1991. Regional Geology of Nei Mongolia Autonomous Region. Geological Publishing House, Beijing (in Chinese with English abstract).
Carlson, W.D., Donelick, R.A., Ketcham, R.A., 1999. Variability of apatite fission-track annealing kinetics: I. Experimental results. American Mineralogist 84, 1213–1223.
Deng, J.F., Mo, X.X., Zhao, H.L., 2004. A new model for the dynamic evolution of Chinese lithosphere: continental root plume tectonics. Earth Science Reviews 65, 223–275.
Dunkl, I., 2002. TRACKKEY: a Windows program for calculation and graphical presentation of fission track data. Computers & Geosciences 28, 3–12.
Engebretson, D.C., Cox, A., Gordon, R.G., 1985. Relative motions between oceanic and continental plates in the Pacific basins. Geological Society of America, Special Paper 206, 1–59.
England, P., Molnar, P., 1990. Surface uplift, uplift of rocks, and exhumation of rocks. Geology 18, 1173–1177.
Fan, W.M., Guo, F., Wang, Y.J., Lin, G., 2003. Calc-alkaline volcanism of post-orogenic extension in the northern Da Hinggan Mountains, northeastern China. Journal of Volcanology and Geothermal Research 121, 115–135.
Fitzgerald, P.G., Stump, E., 1997. Cretaceous and Cenozoic episodic denudation of the Transantarctic Mountains, Antarctica: new constraints from apatite fission track thermochronology in the Scott Glacier region. Journal of Geophysical Research 102, 7747–7765.
Gallagher, K., Brown, R., Johnson, C., 1998. Fission track analysis and its application to geological problems. Annual Review of Earth and Planetary Sciences 26, 519–572.
Ge, W.C., Lin, Q., Sun, D.Y., 1999. Geochemical characteristics of the Mesozoic basalts in Da Hinggan Ling Evidence of the mantle–crust interaction. Acta Petrologica Sinica 15, 396–407 (in Chinese with English abstract).
Gleadow, A.J.W., 1981. Fission-track dating methods: what are the real alternatives? Nuclear Tracks 5, 3–14.
Gleadow, A.J.W., Fitzgerald, P.G., 1987. Uplift history and structure of the Transantarctic Mountains: new evidence from fission track dating of basement apatites in the Dry Valleys area, southern Victoria Land. Earth and Planetary Science Letters 82, 1–14.
Gleadow, A.J.W., Hurford, A.J., Quaife, R.D., 1976. Fission track dating of zircon: improved techniques. Earth and Planetary Science Letters 33, 273–276.
Grimmer, J.C., Jonckheere, R., Enkelmann, E., Ratschbacher, L., Hacker, B.R., Blythe, A.E., Wagner, G.A., Wu, Q., Liu, S., Dong, S., 2002. Cretaceous–Cenozoic history of the southern Tan-Lu fault zone: apatite fission-track and structural constraints from the Dabie Shan (eastern China). Tectonophysics 359, 225–253.
Guo, F., Nakamura, E., Fan, W.M., Kobayoshi, K., Li, C.W., 2007. Generation of Palaeocene adakitic andesites by magma mixing; Yanji Area, NE China. Journal of Petrology 48, 661–692.
Hong, D.W., Zhang, J.S., Wang, T., Wang, S.G., Xie, X.L., 2004. Continental crustal growth and the supercontinental cycle: evidence from the Central Asian Orogenic Belt. Journal of Asian Earth Sciences 23, 799–813.

Hurford, A.J., Green, P.F., 1983. The Zeta age calibration of fission-track dating. Isotope Geoscience 1, 285–317.
Hurford, A.J., 1990. Standarization of fission track dating calibration: recommendation by the Fission Track Working Group of the IUGS Subcommission on Geochronology. Chemical Geology 180, 171–178.
Jahn, B.M., Wu, F.Y., Capdevila, R., Fourcade, S., Wang, Y.X., Zhao, Z.H., 2001. Highly evolved juvenile granites with tetrad REE patterns: the Woduhe and Baerzhe granites from the Great Xing'an (Khingan) Mountains in NE China. Lithos 59, 171–198.
Jia, D.C., Hu, R.Z., Lu, Y., Qiu, X.L., 2004. Collision belt between the Khanka block and the North China block in the Yanbian Region, Northeast China. Journal of Asian Earth Sciences 23, 211–219.
Johnson, C., 1997. Resolving denudational histories in orogenic belts with apatite fission track thermochronology and structural data: an example from southern Spain. Geology 25, 623–625.
Kemp, P.J.J., 1989. Fission track analysis reveals character of collisional tectonics. Tectonics 8, 169–195.
Ketcham, R.A., 2005. Forward and inverse modeling of low-temperature thermochronometry data. Reviews in Mineralogy & Geochemistry 58, 275–314.
Ketcham, R.A., Carter, A., Donelick, R.A., Barbarand, J., Hurford, A.J., 2007a. Improved measurement of fission-track annealing in apatite using *c*-axis projection. American Mineralogist 92, 789–798.
Ketcham, R.A., Carter, A., Donelick, R.A., Barbarand, J., Hurford, A.J., 2007b. Improved modeling of fission-track annealing in apatite. American Mineralogist 92, 799–810.
Lapierre, H., Jahn, B.M., Charvet, J., Yu, Y.W., 1997. Mesozoic felsic arc magmatism and continental olivine tholeiites in Zhejiang Province and their relationship with the tectonic activity in southeastern China. Tectonophysics 274, 321–338.
Lei, J., Zhao, D., 2005. P-wave tomography and origin of the Changbai intraplate volcano in Northeast Asia. Tectonophysics 397, 281–295.
Li, J.Y., 2006. Permian geodynamic setting of Northeast China and adjacent regions: closure of the Paleo-Asian Ocean and subduction of the Paleo-Pacific Plate. Journal of Asian Earth Sciences 26, 207–224.
Li, X.H., 2000. Cretaceous magmatism and lithospheric extension in Southeast China. Journal of Asian Earth Sciences 18, 293–305.
Li, X.M., Gong, G.L., in press. Late Mesozoic–Cenozoic exhumation history of the Lesser Hinggan Mountains, NE China, revealed by fission track thermochronology. Geological Journal, doi: 10.1002/gj.1267.
Li, X.M., Gong, G.L., Yang, X.Y., Zeng, Q.S., 2010. Late Cretaceous–Cenozoic exhumation of the Yanji area, NE China: constraints from fission track thermochronology. Island Arc 19, 120–133.
Li, Z.X., Li, X.H., 2007. Formation of the 1300-km-wide intracontinental orogen and postorogenic magmatic province in Mesozoic South China: a flat-slab subduction model. Geology 35, 179–182.
Lin, Q., Ge, W.C., Sun, D.Y., Wu, F.Y., Won, C.K., Min, K.D., Jin, M.S., Lee, M.W., Kwon, C.S., Yun, S.H., 1998. Tectonic significance of Mesozoic volcanic rocks in northeastern China. Scientia Geologica Sinica 32 (3), 129–139 (in Chinese with English abstract).
Liu, J.M., Zhang, R., Zhang, Q.Z., 2004. The regional metallogeny of Da Hinggan Ling, China. Earth Science Frontiers 11 (1), 269–277 (in Chinese with English abstract).
Liu, J.Q., Han, J.T., Fyfe, W.S., 2001. Cenozoic episodic volcanism and continental rifting in northeast China and possible link to Japan Sea development as revealed from K–Ar geochronology. Tectonophysics 339, 385–401.
Liu, R.X., Chen, W.J., Sun, J.Z., Li, D.M., 1992. The K–Ar age and tectonic environment of Cenozoic volcanic rocks in China. In: Liu, R.X. (Ed.), The Age and Geochemistry of Cenozoic Volcanic Rock in China. Seismology Press, Beijing, pp. 1–43 (in Chinese).
Ma, X.H., Yang, Z.Y., 1993. The collision and suturing of the three major blocks in China and the reconstruction of the Paleo-Eurasia continent. Acta Geophysica Sinica 36, 476–488 (in Chinese with English abstract).
Meng, Q.R., 2003. What drove Late Mesozoic extension of the northern China–Mongolia tract? Tectonophysics 369, 155–174.
Nakamura, E., McCulloch, M.T., Campbell, I.H., 1990. Chemical geodynamics in the back-arc region of Japan based on the trace element and Sr–Nd isotopic compositions. Tectonophysics 174, 207–233.
Northrup, C.J., Royden, L.H., Burchfiel, B.C., 1995. Motion of the Pacific plate relative to Euroasia and its potential relation to Cenozoic extrusion along the eastern margin of Eurasia. Geology 23, 719–722.
Ren, Z.L., 1999. Study on tectono-thermal histories of sedimentary basins in the north China. Petroleum Industry Press, Beijing (in Chinese).
Roden-Tice, M.K., Tice, S.J., Schofield, I.S., 2000. Evidence for differential unroofing in the Adirondack Mountains, New York State, determined by apatite fission-track thermochronology. Journal of Geology 108, 155–169.
Sengör, A.M.C., Natal'in, B.A., Burtman, V.S., 1993. Evolution of the Altaid tectonic collage and Paleozoic crustal growth in Eurasia. Nature 364, 299–307.
Shao, J.A., Gai, F.Y., Zhang, L.Q., 1998a. Coupling of mantle-upwelling and shearing – mesozoic dyke-swarm in Da Hinggan Mountains, Northeast China. Episodes 21 (2), 99–103.
Shao, J.A., Zhang, L.Q., Mu, B.L., 1998b. Thermo-tectonic evolution in middle and south part of Dahinggan. Science in China Series D 28, 194–200.
Shao, J.A., Zhang, L.Q., Mu, B.L., 1999. Magmatism in the Mesozoic extending orogenic process of Da Hinggan Mts. Earth Science Frontiers 6, 339–346 (in Chinese with English abstract).
Shao, J.A., Zhang, L.Q., Xiao, Q.H., Li, X.B., 2005. Rising of Da Hinggan Mts. in Mesozoic: a possible mechanism of intracontinental orogeny. Acta Petrologica Sinica 21, 789–794 (in Chinese with English abstract).
Sun, D.Y., Wu, F.Y., Li, H.M., Lin, Q., 2001. Emplacement age of the postorogenic A-type granites in Northwestern Lesser Xing'an Ranges, and its relationship to the eastward extension of Suolunshan-Hegenshan-Zhalaite collisional suture zone. Chinese Science Bulletin 46, 427–432.
Sun, W.D., Ding, X., Hu, Y.H., Li, X.H., 2007. The golden transformation of the Cretaceous plate subduction in the west Pacific. Earth and Planetary Science Letters 262, 533–542.
Taira, A., 2001. Tectonic evolution of the Japanese island arc system. Annual Review of Earth and Planetary Sciences 29, 109–134.
Tinker, J., de Wit, M., Brown, R., 2008. Mesozoic exhumation of the southern Cape, South Africa, quantified using apatite fission track thermochronology. Tectonophysics 455, 77–93.
Van der Voo, R., Spakman, W., Bijwaard, H., 1999. Mesozoic subducted slabs under Siberia. Nature 397, 246–249.
Vassallo, R., Jolivet, M., Ritz, J.F., Braucher, R., Larroque, C., Sue, C., Todbileg, M., Javkhlanbold, D., 2007. Uplift age and rates of the Gurvan Bogd system (Gobi-Altay) by apatite fission track analysis. Earth and Planetary Science Letters 259, 333–346.
Wagner, G.A., Van den haute, P., 1992. Fission-track Dating. Enke Verlag, Stuttgart.
Wang, F., Zhou, X.H., Zhang, L.C., Ying, J.F., Zhang, Y.T., Wu, F.Y., Zhu, R.X., 2006. Late Mesozoic volcanism in the Great Xing'an Range (NE China): timing and implications for the dynamic setting of NE Asia. Earth and Planetary Science Letters 251, 179–198.
Wang, P.J., Liu, W.Z., Wang, S.X., Song, W.H., 2002. $^{40}Ar/^{39}Ar$ and K/Ar dating on the volcanic rocks in the Songliao basin, NE China: constraints on stratigraphy and basin dynamics. International Journal of Earth Sciences 91, 331–340.
Wang, Q., Li, S., Du, Z., 2009. Differential uplift of the Chinese Tianshan since the Cretaceous: constraints from sedimentary petrography and apatite fission-track dating. International Journal of Earth Sciences 98, 1341–1363.
Willett, S.D., Fisher, D., Fuller, C., Yeh, E.C., Lu, C.Y., 2003. Erosion rates and orogenic-wedge kinematics in Taiwan inferred from fission-track thermochronometry. Geology 31, 945–948.
Wu, F.Y., Jahn, B.M., Wilde, S.A., Lo, C.H., Yui, T.F., Lin, Q., Ge, W.C., Sun, D.Y., 2003. Highly fractionated I-type granites in NE China (I): geochronology and petrogenesis. Lithos 66, 241–273.
Wu, F.Y., Jahn, B.M., Wilde, S.A., Sun, D.Y., 2000. Phanerozoic continental crustal growth: U–Pb and Sr–Nd isotopic evidence from the granites in northeastern China. Tectonophysics 328, 89–113.
Wu, F.Y., Sun, D.Y., Li, H.M., Iahn, B.M., Wilde, S.A., 2002. A-type granites in northeastern China: Age and geochemical constraints on their petrogenesis. Chemical Geology 187, 143–173.
Wu, F.Y., Lin, J.Q., Wilde, S.A., Sun, D.Y., Yang, J.H., 2005. Nature and significance of the Early Cretaceous giant igneous event in eastern China. Earth and Planetary Science Letters 233, 103–119.
Wu, F.Y., Sun, D.Y., Ge, W.C., Zhang, Y.B., Grant, M.L., Wilde, S.A., Jahn, B.M., 2011. Geochronology of the Phanerozoic granitoids in northeastern China. Journal of Asian Earth Sciences 41, 1–30.
Xiang, C.F., Feng, Z.Q., Pang, X.Q., Wu, H.Y., Li, J.H., 2007. Late stage thermal history of the Songliao Basin and its tectonic implications: evidence from apatite fission track (AFT) analyses. Science in China Series D 50, 1479–1487.
Xiao, W.J., Windley, B., Hao, J., Zhai, M.G., 2003. Accretion leading to collision and the Permian Solonker suture, Inner Mongolia, China: termination of the Central Asian Orogenic Belt. Tectonics 22 (6), 1069. doi:10.1029/2002TC001484.
Xu, X.S., Dong, C.W., Li, W.X., Zhou, X.M., 1999. Late Mesozoic intrusive complexes in the coastal area of Fujian, SE China: the significance of the gabbro-diorite – granite association. Lithos 46, 299–315.
Xu, Y.G., 2007. Diachronous lithospheric thinning of the North China Craton and formation of the Daxin'anling–Taihangshan gravity lineament. Lithos 96, 281–298.
Yin, C.J., Peng, Y.J., Jin, K., 2000. Mesozoic volcanism in the eastern part of Northeast China and Transpacific plate. Regional Geology of China 19, 303–311 (in Chinese with English abstract).
Yuan, W.M., Carter, A., Dong, J.Q., Bao, Z.K., An, Y.C., Guo, Z.J., 2006. Mesozoic-Tertiary exhumation history of the Altai Mountains, northern Xinjiang, China: new constraints from apatite fission track data. Tectonophysics 412, 183–193.
Zhao, X.X., Coe, R.S., 1996. Paleomagnetic Constraints on the Paleogeography of China: Implications for Gondwanaland. Abstract of 30th IGC, vol. 1, p. 231.
Zhao, X.X., Coe, R.S., Zhou, Y.X.S., Wu, H.R., Wang, J., 1990. New palaeomagnetic results from northern China: collision and suturing with Siberia and Kazakhstan. Tectonophysics 181, 43–81.
Zhao, Y., Yang, Z.Y., Ma, X.H., 1994. Geotectonic transition from Paleoasian system and Paleotethyan system to Paleopacific active continental margin in eastern Asia. Scientia Geologica Sinica 29, 105–119 (in Chinese with English abstract).
Zhou, X.M., Li, W.X., 2000. Origin of Late Mesozoic igneous rocks in Southeastern China: implications for lithosphere subduction and underplating of mafic magmas. Tectonophysics 326, 269–287.
Zonenshain, L.P., Kuzmin, M.I., Natapov, L.M., 1990. Geology of the USSR: a plate-tectonic synthesis. In: Page, B.M. (Ed.), AGU Geodynamics Series, vol. 21, pp. 242.